ELSEVIER

International Journal of Minerals, Metallurgy and Materials
Volume 16, Number 4, August 2009, Page 407

Materials

Effect of hydrogen on the stress corrosion cracking behavior of X80 pipeline steel in Ku'erle soil simulated solution

Ping Liang[1,2], *Cui-wei Du*[1], *Xiao-gang Li*[1], *Xu Chen*[1], *and Zhang liang*[1]

1) School of Materials Science and Engineering, University of Science and Technology Beijing, Beijing 100083, China
2) School of Mechanical Engineering, Liaoning Shihua University, Fushun 113001, China
(Received 2008-06-19)

Abstract: Hydrogen was a key factor resulting in stress corrosion cracking (SCC) of X80 pipeline steel in Ku'erle soil simulated solution. In this article, the effect of hydrogen on the SCC susceptibility of X80 steel was investigated further by slow strain rate tensile test, the surface fractures were observed using scanning electron microscopy (SEM), and the fracture mechanism of SCC was discussed. The results indicate that hydrogen increases the SCC susceptibility. The SEM micrographs of hydrogen precharged samples presents a brittle quasi-cleavage feature, and pits facilitate the transgranular crack initiation. In the electrochemical impedance spectroscopy (EIS) measurement, the decreased polarization resistance and the pitting resistance of samples with hydrogen indicate that hydrogen increases the dissolution rate and deteriorates the pitting corrosion resistance. The potentiodynamic polarization curves present that hydrogen also accelerates the dissolution rate of the crack tip.

Key words: pipeline steel; stress corrosion cracking; hydrogen assisted cracking; slow strain rate tensile

[*The work was financially supported by the National Science & Technology Infrastructure Development Program of China (No.2005DKA10400).*]

1. Introduction

Stress corrosion cracking (SCC) can be defined as an interaction of tensile stress and corrosion environment acting on a susceptible metallic surface to initiate and propagate cracks [1]. SCC is localized corrosion, as well as causes grave damage that affects the service safety of pipeline steel. Since 1965, SCC has occurred in several countries throughout the world and contributed to major failures in some high-pressure natural gas transmission pipelines [2-3].

It has been acknowledged [4-5] that there are two basic forms of SCC on the external surface of buried pipeline steels: high pH-SCC and low pH-SCC. High pH-SCC [6-7] is characterized by numerous shallow and longitudinal intergranular cracks. The growth rate of a crack increases exponentially with temperature and stress. Cracking is related to a concentrated alkaline electrolyte (approximately pH=9.0) in contact with the steel surface. It has been suggested that the simulated solution for high pH-SCC in the laboratory is 1 mol $NaHCO_3$+0.5 mol Na_2CO_3. The passive film rupture and anodic metal dissolution at the crack tip can be assigned to the mechanism of SCC in the high pH electrolyte [8]. Reducing the pipe temperature and controlling the pipe electrochemical potential range may possibly reduce or avoid the emergence of high pH-SCC. The latter, near-neutral SCC, was first discovered in Canada in the early 1980s [9]. This form of SCC propagates transgranularly and has no obvious correlation with temperature. It takes place in a dilute solution, with the pH range from 5.5 to 8.5, and NS4 solution (0.122 $g \cdot L^{-1}$ KCl, 0.483 $g \cdot L^{-1}$ $NaHCO_3$, 0.181 $g \cdot L^{-1}$ $CaCl_2 \cdot 2H_2O$, 0.131 $g \cdot L^{-1}$ $MgSO_4 \cdot 7H_2O$) is used normally as the simulated solution, in the laboratory [10]. The mechanism of near-neutral SCC has not been well understood, and some literatures proposed [11-12] the cracking process resulting from a possible synergistic effect between anodic dissolution and hydrogen that entered into the steel.

X80 pipeline steel, which has high-intensity and high-toughness, is a low carbon, micro-alloyed,

Corresponding author: Ping Liang, **E-mail:** liangping770101@163.com

Also available online at www.sciencedirect.com

high-grade steel, and is relatively new as a pipeline material in China and in other countries. The material will be applied widely for building gas transmission pipelines in the 21th century [13]. Ku'erle region in north-western China is abundant in natural gas resources, and a great number of gas pipelines are buried in this place. In view of the disaster of SCC and the importance of pipeline network safety during service, it is crucial to investigate the SCC susceptibility of X80 steel in this environment. Moreover, the wide use of cathodic protection systems on buried pipelines does increase the likelihood of SCC [14-15]. In this laboratory, an experimental result [16] inferred that the SCC of X80 steel in a simulated solution, based on the chemistry of Ku'erle soil, was related to the hydrogen produced from the corrosion process. Therefore, this article was aimed at evaluating the effect of hydrogen on the SCC tendency of X80 steel in Ku'erle soil simulated solution by slow strain rate test.

2. Experimental

2.1. Experimental material and solution

X80 pipeline steel was used as the experimental material in this study. Its chemical composition is listed in Table 1, and the surface microstructure is shown in Fig. 1. It was observed that X80 steel exhibited a uniform acicular ferrite structure.

Table 1. Chemical composition of X80 pipeline steel wt%

C	Mn	P	S	Si	Cu	Al	Ti	Cr
0.041	1.67	0.01	0.0006	0.196	0.258	0.0421	0.011	0.031
Ca	Pb	Sb	Sn	As	B	Ni	Nb	Fe
0.0017	0.0028	0.0031	0.0048	0.007	0.003	0.246	0.095	Bal.

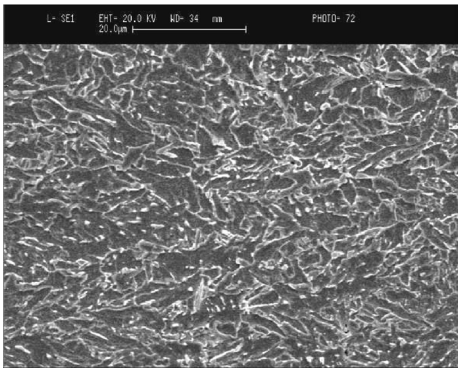

Fig. 1. Microstructure of X80 pipeline steel.

Table 2 gives the chemical composition of Ku'erle soil simulated (synthetic) solution, which is based on the average contents of soil samples. The pH was adjusted to 9.0±0.2 using sodium hydroxide (NaOH). All solutions were prepared by mixing analytical grade reagents with deionized water. The temperature was controlled at 25±2°C during all experiments. Deaeration of the test solution was achieved by purging the solution with nitrogen gas for 2 h prior to the test, and then purging was continued during all the slow strain rate tests.

Table 2. Chemical composition of a synthetic solution simulated the soil composition of Ku'erle region g/L

$NaHCO_3$	KNO_3	Na_2SO_4	$CaCl_2$	NaCl	$MgCl_2{\cdot}6H_2O$
0.1462	0.2156	2.5276	0.2442	3.1707	0.6699

2.2. Potentiodynamic polarization and electrochemical impedance spectroscopy (EIS) measurements

The electrochemical experiments were carried out in a three-electrode cell system, in which a saturated calomel electrode (SCE) was used as the reference electrode and a platinum sheet as the counter electrode. It should be noted that all potentials quoted in this article were referred to SCE.

The specimens were immersed in deoxygenated synthetic solution at the open circuit potential (OCP) for 0.5 h prior to potentiodynamic polarization measurements. The polarization curve was obtained using EG&G 2273 at a scanning rate of 1000 mV/min. EIS measurements were carried out with the AC amplitude of the sinusoidal perturbation of 10 mV and the measurement frequency from 100 kHz down to 10 mHz.

2.3. Slow strain rate tensile tests (SSRT)

The stress corrosion cracking susceptibility of X80 steel in the synthetic solution was evaluated using the SSRT method. Tensile smooth plate specimens (gauge length: 32 mm; gauge thickness: 2 mm; and gauge width: 6 mm) were made in the longitudinal direction. Prior to testing, the gauge lengths of the specimens were polished with 1000 grit emery paper along the tensile direction, degreased with acetone in an ultrasonic cleaner, washed with distilled water, and finally dried in air. The strain rate was controlled at 1×10^{-6} s^{-1}. The SCC susceptibility was expressed in terms of the percentage change in the reduction in area (RA). The lower the RA, the higher the SCC susceptibility, RA is calculated by the following equation:

$$\mathrm{RA}=\frac{S_0-S_\mathrm{A}}{S_0}\times100\% \quad (1)$$

where S_0 is the initial area of the tensile specimen, and

S_A is the final fracture area of the tensile specimen.

2.4. Fracture surface analysis

After SSRT tests, the specimens were cleaned in 500 mL HCl+500 mL H_2O+10 g hexamethylenetetramine for 3-5 min to remove the corrosion product, and then dipped in acetone for 5 min. The fracture surfaces of various samples were observed by scanning electron microscopy (SEM).

3. Results

3.1. Effect of potential on the SCC of X80 steel

Fig. 2 shows the stress-strain curves of X80 steel in air, at the open circuit potential (OCP, −725.0 mV), and at −1200 mV in Ku'erle soil simulated solution. In air, the time of fracture (t_f) and the percentage of RA were 48.37 h and 68.22%, respectively. The data could be used as a standard against that obtained in the solution. When the X80 steel sample was carried out at OCP, the values of t_f and RA were 41.04 h and 53.58%, respectively, which were lower than those obtained in air. This indicated that the synthetic solution condition assisted X80 steel cracking and had the tendency for SCC. At −1200 mV, t_f and RA decreased to 31.43 h and 21.25%, respectively. These values decreased obviously as compared with those obtained in air and at OCP. It meant that the more negative the potentials, the higher the SCC susceptibility. It was probably a result of the ingress of hydrogen into the steel under the experimental condition.

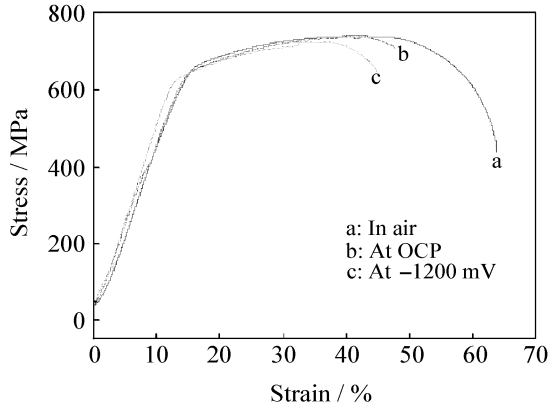

Fig. 2. Stress-strain curves of X80 steel in air and in Ku'erle soil simulated solution.

From the chemical composition of Ku'erle soil simulated solution (seen Table 2), it can be seen that the levels of Cl^- and SO_4^{2-} were relatively high, with pH close to 9.0. According to this, some main electrochemical reactions in the deoxygenated solution can be deduced as

$$Fe \rightarrow Fe^{2+} + 2e \quad (2)$$

$$H_2O \rightarrow H^+ + OH^- \quad (3)$$

$$H^+ + e \rightarrow H \quad (4)$$

$$H + H \rightarrow H_2 \quad (5)$$

Owing to hydrogen ion reduction to absorbed atoms, the potential could be expressed by $E_H = -0.059$ pH = −531 mV *vs.* standard hydrogen electrode (SHE) = −775 mV *vs.* SCE. However, an ohmic drop was caused by the complicated chemical compositions of simulated solution [5], thus, a part of the applied cathode potential was consumed. Therefore, a more negative potential than −775 mV *vs.* SCE for hydrogen ion reduction would be required in the synthetic solution. When the potential was −1200 mV *vs.* SCE, hydrogen began to evolve, entered the specimen, and subsequently accumulated in the crack tip during the process of SCC. The interaction of hydrogen and tensile stress resulted in the increase of SCC susceptibility.

SEM fracture morphologies of X80 steel specimens after SSRT in air, at OCP and at −1200 mV are shown in Fig. 3. Ductile failure as revealed by a significant extent of dimples was found on the fractured surface of specimens tested in air (Fig. 3(a)) and at OCP (Fig. 3(b)), which manifested that the X80 steel used in this study was slightly susceptible to SCC in the simulated solution at OCP. However, at −1200 mV, an obvious brittle quasi-cleavage cracking morphology was exhibited, as shown in Fig. 3(c). It meant that the SCC susceptibility of X80 steel in Ku'erle soil simulated solution increased greatly at this potential.

3.2. Effect of precharged hydrogen time on the SCC of X80 steel

To study the effect of hydrogen on SCC, the X80 steel specimens were precharged with hydrogen at a current density of 20 mA/cm^2 for 24 h and 48 h before straining. Fig. 4 presents the stress-strain curves of X80 steel at −1200 mV in this simulated solution with various precharged hydrogen time. The values of RA and t_f are presented in Fig. 5. It could be seen from the results that a significant reduction in t_f and RA was observed for the precharged specimens, which implied that the SCC susceptibility of X80 steel increased with the prolongation of charging time. It was because in case of the precharged specimens, despite part of the hydrogen escaping from the specimens during SSRT, the hydrogen concentration in X80 steel was higher for a longer precharged time. Obviously, the higher the hydrogen concentration in X80 steel, the more the hydrogen concentrated at the crack tip.

SEM micrographs of the fracture surfaces of X80 steel after SSRT are shown in Fig. 6. It seemed as if the fracture surfaces of both the specimens exhibited

obvious brittle 'quasi-cleavage-like' fracture cracking features, which were often associated with hydrogen induced cracking [17-18]. In addition, there were also secondary cracks in the hydrogen-charged specimens. Takano [19] also observed a similar fracture surface morphology in a 7075 aluminum alloy, which was cathodically charged. He also suggested that such fractures resulted from the accumulation of hydrogen.

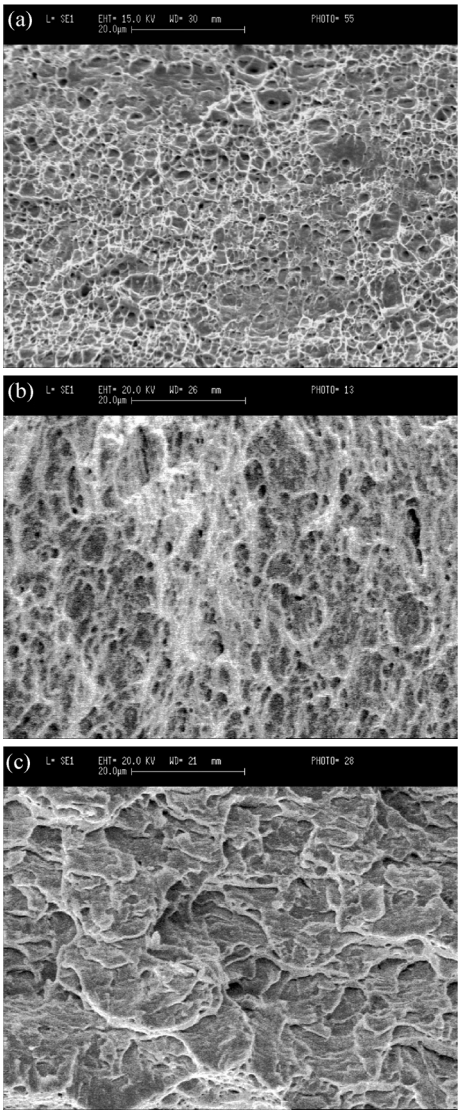

Fig. 3. SEM micrographs of the fracture surfaces of X80 steel in Ku'erle soil simulated solution: (a) in air; (b) at OCP; (c) at −1200 mV.

The SEM micrographs of the lateral surface near the fracture section of the unprecharged and precharged hydrogen samples are shown in Fig. 7. From graphs, it could be seen that the principal fracture path in X80 steel specimens tended to be parallel to the rolling plane (perpendicular to the applied stress). It also seemed significant that both the number and the length of transgranular microcracks were more in the precharged hydrogen specimen. The results meant that hydrogen in X80 steel promoted crack propagation and facilitated SCC, which was also a further indication of the entry of hydrogen into the steel. In addition, some cracks appeared to initiate from some corrosive pits, as seen in Fig. 7(d).

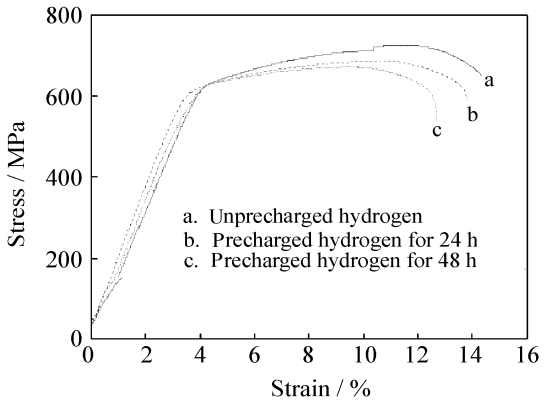

Fig. 4. Effect of precharged time on the stress-strain curves of X80 steel at −1200 mV in Ku'erle soil simulated solution.

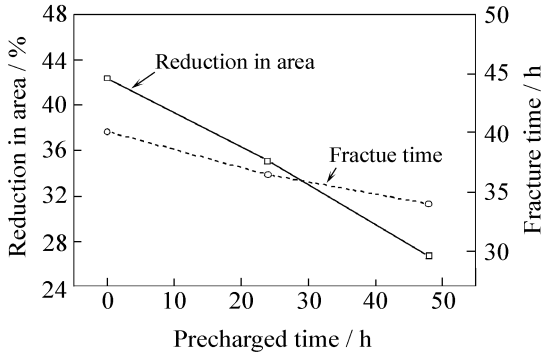

Fig. 5. Effect of precharged time on the RA and t_f of X80 steel tested in Ku'erle soil simulated solution.

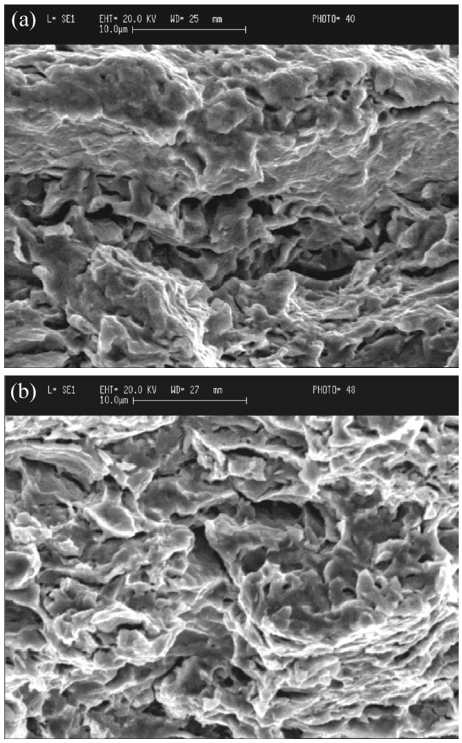

Fig. 6. SEM micrographs of the fracture surfaces of X80 steel tested at −1200 mV in simulated solution (precharged hydrogen at 20 mA/cm^2): (a) 24 h; (b) 48 h.

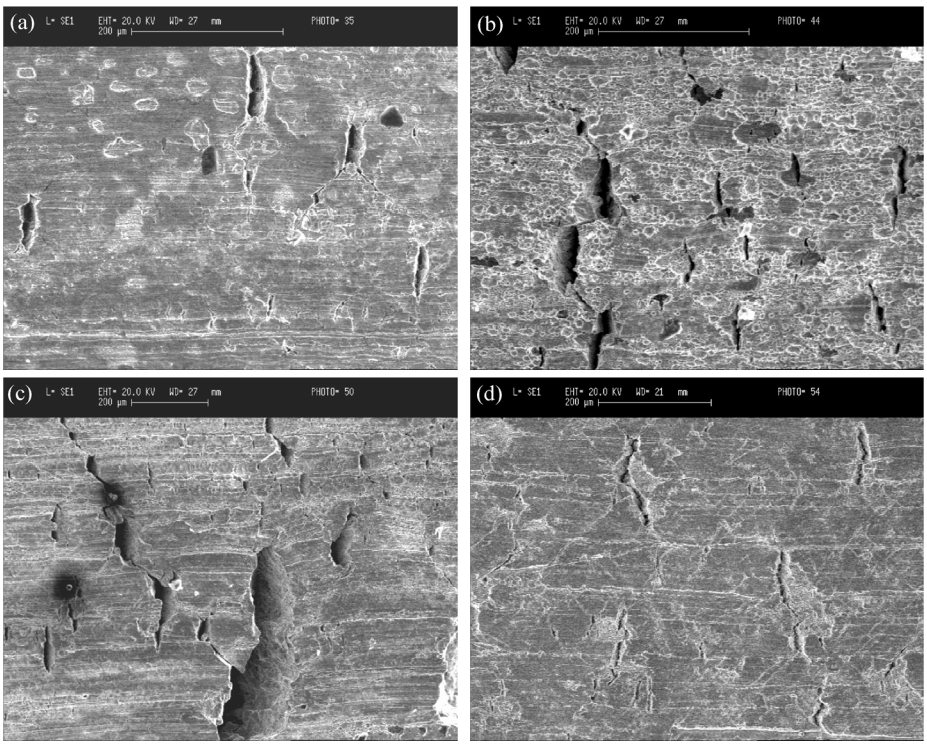

Fig. 7. SEM micrographs of the lateral surfaces near the fracture of X80 steel in Ku'erle soil simulated solution at −1200 mV: (a) unprecharged; (b) precharged for 24 h; (c) precharged for 48 h; (d) cracks initiated from pitting.

4. Discussion

From the above analysis, it could be concluded that hydrogen increased the SCC susceptibility of X80 steel in the simulated solution. Moreover, it was also observed that the crack density was more in the precharged than the unprecharged hydrogen specimens, and some cracks evolved in the interior of the pits. Therefore, it led to the conclusion that the pits were a precursor to SCC for X80 steel in the simulated solution. To confirm this, the effect of hydrogen on the pitting behavior was investigated.

4.1. Effect of hydrogen on pitting corrosion

In order to study the effect of hydrogen on the pitting corrosion behavior in more detail, EIS measurements were performed. Fig. 8 shows the impedance spectra for the samples measured in Ku'erle soil simulated solution, where Z_{Re} is the real part of impedance, and Z_{Im} is the imaginary part of impedance. Prior to the EIS measurements, the samples were precharged with hydrogen at 20 mA/cm^2 for 1 h and 3 h, respectively.

The equivalent circuit is shown in Fig. 9, where R_s is the solution resistance, C_{dl} is the double layer capacity, R_p is the polarization resistance, R_{pit} and C_{pit} are the resistance and capacitance for the pitting [20]. The fitting results are listed in Table 3. Compared with the unprecharged hydrogen specimens, the capacity arc for the precharged specimens obviously decreased. Moreover, the longer the precharged time, the smaller the capacitive arc. Table 3 indicated that R_p and R_{pit} decreased, whereas, C_{dl} and C_{pit} increased because of hydrogen. The effect became more obvious with an increase in precharged hydrogen time. Since R_{pit} was related to the anodic dissolution rate at the pitting area [20], the clear decrease of R_{pit} implied that hydrogen had the ability to accelerate pitting initiation on X80 steel.

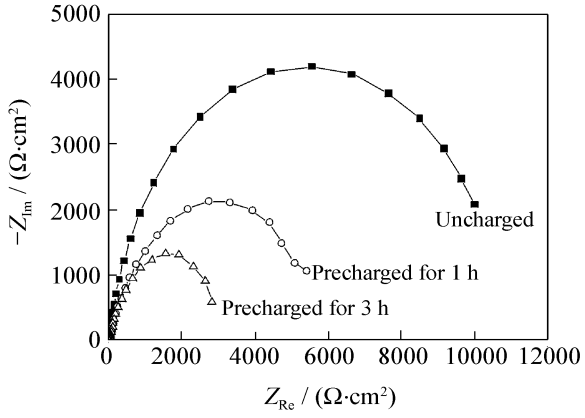

Fig. 8. Impedance spectra for X80 steel in Ku'erle simulated solution at open circuit potential, the specimens were precharged at 20 mA/cm^2.

Fig. 10 shows that the optical microscopy of X80 steel precharged at a current density of 20 mA/cm^2 for 1 h and 3 h, respectively. It could be seen that a lot of pits appeared on the surface, and the number of pits increased with the delay of precharged time. Hence, it

confirmed the assumption that hydrogen promoted pitting. Lots of these pits might form preferential initiation sites for SCC during SSRT tests. Moreover, a low pH environment might come into being in some deep pits [21], which was helpful for the production and accumulation of hydrogen atoms, and this might accelerate the local microplastic deformation and facilitate crack nucleation and propagation. As a result, brittle cracks occurred.

4.2. Effect of hydrogen on the polarization curves

Parkins [22-23] suggested that the corrosion rate of the crack tip could be expressed by the polarization curves at a quick scan rate, and the current density was caused by metal dissolution. To understand the effect of hydrogen on the crack tip, potentiodynamic polarization was carried out at a scan rate of 1000 mV/min for the unprecharged and precharged hydrogen specimens. The results are shown in Fig. 11, where E is the corrosion potential, and i is the corrosion density. The fitting results for the corrosion current potential (E_{corr}) and corrosion current density (i_{corr}) are listed in Table 4. The charged specimens exhibited a lower i_{corr} than that of the uncharged, and the i_{corr} increased with increasing exposure time. In addition, the E_{corr} was also notably decreased by hydrogen. These indicated that hydrogen increased the dissolution rate of the crack tip.

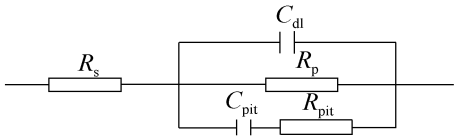

Fig. 9. Equivalent circuit for X80 steel precharged with hydrogen at 20 mA/cm^2 for 1 h and 3 h in Ku'erle simulated solution at open circuit potential.

Table 3. Impedance fitting parameters obtained for unprecharged and precharged hydrogen of X80 steel in Ku'erle simulated solution

Precharged hydrogen time / h	R_s / (Ω·cm^2)	C_{dl} / (F·cm^{-2})	R_p / (Ω·cm^2)	C_{pit} / (F·cm^{-2})	R_{pit} / (Ω·cm^2)
0	17.27	4.785×10^{-5}	9451	3.694×10^{-5}	1001.0
1	22.87	6.199×10^{-5}	4859	9.871×10^{-5}	449.2
3	16.35	2.103×10^{-5}	2716	3.615×10^{-5}	324.6

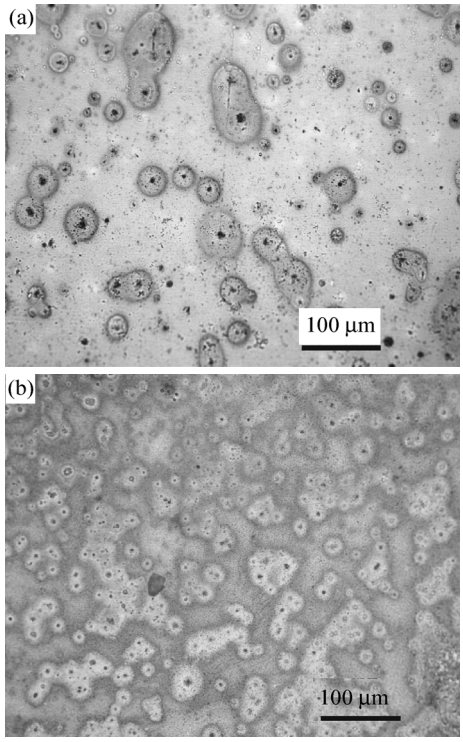

Fig. 10. Optical microscopy of X80 steel was precharged hydrogen at 20 mA/cm^2 for different time intervals: (a) 1 h; (b) 3 h.

From the results of EIS and polarization curves, it could be seen that hydrogen increased the pitting behavior of X80 steel, and accelerated the dissolution rate of the crack tip. Therefore, it could be deduced that when the potential was −1200 mV, the hydrogen atoms would produce and enter into X80 steel.

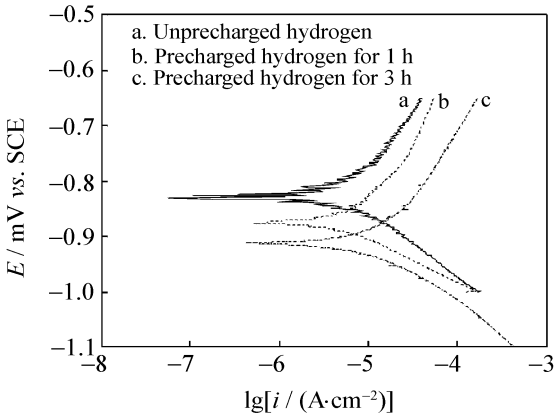

Fig. 11. Potentiodynamic polarization curves of X80 steel specimens in Ku'erle simulated solution precharged with hydrogen at 20 mA/cm^2 at a scan rate of 1000 mV/min.

When the hydrogen concentration at the crack tip was above a critical value, the steel got brittle. Therefore, with the delay of precharged hydrogen time, more hydrogen atoms entered into the steel. This led to two results. On the one hand, the corrosive pits increased. Undoubtedly, a part of the pits facilitated crack initiation by notching effect yielding to an increase of stress at the pit bottom. On the other hand, when the cracks initiated, the hydrogen that entered into X80 steel would concentrate at the crack tip dur-

ing the SCC process. Hydrogen might cause internal energy change and entropy change of X80 steel, and could interact with stress. These changes resulted in an increase in anodic dissolution rate. Therefore, the SCC susceptibility of X80 steel in the simulated solution increased.

Table 4. Fitting results of the potentiodynamic polarization curves of X80 steel precharged with hydrogen for different time intervals

X80 steel specimen	E_{corr} / mV *vs.* SCE	i_{corr} / ($\mu A \cdot cm^{-2}$)
Unprecharged hydrogen	−830	6.55
Precharged hydrogen for 1 h	−877	11.39
Precharged hydrogen for 3 h	−911	14.06

5. Conclusions

(1) X80 steel shows little tendency to SCC in Ku'erle soil simulated solution of pH 9.0 at OCP. Ductile failure, as revealed by a significant extent of dimples, is obtained in air and at OCP. However, at −1200 mV, the fracture time and the reduction in area decrease dramatically, which are consistent with SEM observations, and indicate SCC by hydrogen induced cracking.

(2) When the X80 steel specimens are tested at −1200 mV in the simulated solution, the SCC susceptibility increases with the increase in precharged hydrogen time.

(3) Pits are the main cause of initiation of transgranular stress corrosion cracks in X80 steel in soil simulated solution, and hydrogen promotes pitting corrosion and facilitates the dissolution rate of the crack tip.

References

[1] G.V. Boven, W. Chen, and R. Rogge, The role of residual stress in neutral pH stress corrosion cracking of pipeline steels. Part I: Pitting and cracking occurrence, *Acta Mater.*, 55(2007), No.1, p.29.

[2] J.Q. Wang and A. Atrens, SCC initiation for X65 pipeline steel in the high pH carbonate/bicarbonate solution, *Corros. Sci.*, 45(2003), No.10, p.2199.

[3] E. Villalba and A. Atrens, An evaluation of steels subjected to rock bolt SCC conditions, *Eng. Failure Anal.*, 14(2007), No.7, p.1351.

[4] C. Manfredi and J.L. Otegui, Failure by SCC in buried pipelines, *Eng. Failure Anal.*, 9(2002), p.495.

[5] L. Niu and Y.F. Cheng, Corrosion behavior of X-70 pipe steel in near-neutral pH solution, *Appl. Surf. Sci.*, 253(2007), No.21, p.8626.

[6] R.N. Parkins, Mechanistic aspects of intergranular stress corrosion cracking of ferritic steels, *Corrosion*, 52(1996), No.5, p.363.

[7] J. Li, M. Elboujdaini, B. Fang, *et al.*, Microscopy study intergranular stress corrosion cracking of X-52 line pipe steel, *Corrosion*, 62(2006), No.4, p.316.

[8] A.K. Pilkey, S.B. Lambert, and A. Plumtree, Stress corrosion cracking of X-60 line pipe steel in a carbonate-bicarbonate solution, *Corrosion*, 51(1995), No.2, p.91.

[9] Y.F. Cheng, Fundaments of hydrogen evolution reaction and its implications on near-neutral pH stress corrosion cracking of pipelines, *Electrochim. Acta*, 52(2007), No.7, p.2661.

[10] R. Chu, W. Chen, S.H. Wang, *et al.*, Microstructure dependence of stress corrosion cracking initiation in X-65 pipeline steel exposed to a near-neutral pH soil environment, *Corrosion*, 60(2004), p.275.

[11] Y.F. Cheng and L. Niu, Mechanism for hydrogen evolution reaction on pipeline steel in near-neutral pH solution, *Electrochem. Commun.*, 9(2007), No.4, p.558.

[12] W. Chen, F. King, and E. Vokes, Charactreistics of near-neutral-pH stress corrosion cracks in an X-65 pipeline, *Corrosion*, 58(2002), No.3, p.267.

[13] L.J. Zhang, Z. Zhang, F.H. Cao, *et al.*, Sturdy of the X70 pipeline steel corrosion in 3.0wt% NaCl solution using electrochemical impedance spectroscopy technique, *Acta Metall. Sin.*, 17(2004), p.907.

[14] T. Kamimura and H. Kishikawa, Mechanism of cathodic disbonding of three-layer polyethylene-coated steel pipe, *Corrosion*, 54(1998), p.979.

[15] M.C. Yan and Y.J. Weng, Study on hydrogen absorption of pipeline steel under cathodic charging, *Corros. Sci.*, 48(2006), No.2, p.432.

[16] P. Liang, C.W. Du, X.G. Li, *et al.*, Stress corrosion cracking of X80 pipeline steel in simulated alkaline soil solution, *Mater. Des.*, 30(2009), No.5, p.1712.

[17] D. Delafosse and T. Magnin, Hydrogen induced plasticity in stress corrosion cracking of engineering systems, *Eng. Fract. Mech.*, 68(2001), No.6, p.693.

[18] R.N. Parkins, W.K. Blanchard Jr, and B.S. Delanty, Transgranular stress corrosion cracking of high-pressure pipelines in contact with solutions of near neutral pH, *Corrosion*, 50(1994), No.5, p.394.

[19] N. Takano, Hydrogen diffusion and embrittlement in 7075 aluminum alloy, *Mater. Sci. Eng. A*, 483-484(2007), No.15, p.336.

[20] Y.M. Zeng, J.L. Luo, and P.R. Norton, Initiation and propagation of pitting and crevice corrosion of hydrogen-containing passive films on X70 micro-alloyed steel, *Electrochim. Acta*, 49(2004), No.5, p.703.

[21] B. Gu, W.Z. Yu, J.L. Luo, and X. Mao, Transgranular stress corrosion cracking of X-80 and X-52 pipeline steels in dilute aqueous solution with near-neutral pH, *Corrosion*, 55(1999), No.3, p.312.

[22] R.N. Parkins, Predictive approaches to stress corrosion cracking failure, *Corros. Sci.*, 30(1980), No.1, p.147.

[23] M. Blengino, M. Keddam, J.P. Labbe, *et al.*, Physico-chemical characterization of corrosion layers formed on iron in a sodium carbonate-bicarbonate containing environment, *Corros. Sci.*, 37(1995), No.4, p.621.